

## Revisit to the yield ratio of triton and $^3\text{He}$ as an indicator of neutron-rich neck emission

Yijie Wang<sup>a,1</sup>, Mengting Wan<sup>b,c</sup>, Xinyue Diao<sup>a</sup>, Sheng Xiao<sup>a</sup>,  
 Yuhao Qin<sup>a</sup>, Zhi Qin<sup>a</sup>, Dong Guo<sup>a</sup>, Dawei Si<sup>a</sup>, Boyuan Zhang<sup>a</sup>,  
 Baiting Tian<sup>a</sup>, Fenhai Guan<sup>a</sup>, Qianghua Wu<sup>a</sup>, Xianglun Wei<sup>e</sup>,  
 Herun Yang<sup>e</sup>, Peng Ma<sup>e</sup>, Rongjiang Hu<sup>e</sup>, Limin Duan<sup>e</sup>,  
 Fangfang Duan<sup>e</sup>, Junbing Ma<sup>e</sup>, Shiwei Xu<sup>e</sup>, Qiang Hu<sup>e</sup>,  
 Zhen Bai<sup>e</sup>, Yanyun Yang<sup>e</sup>, Jiansong Wang<sup>f,e</sup>, Wenbo Liu<sup>h</sup>,  
 Wanqing Su<sup>h</sup>, Xiaobao Wei<sup>h</sup>, Chunwang Ma<sup>h</sup>, Xinxiang Li<sup>k,i</sup>,  
 Hongwei Wang<sup>i,j</sup>, Yingxun Zhang<sup>l</sup>, Michał Warda<sup>m</sup>,  
 Arthur Dobrowolski<sup>m</sup>, Bożena Nerlo-Pomorska<sup>m</sup>,  
 Krzysztof Pomorski<sup>m</sup>, Li Ou<sup>b,c,2</sup>, Zhigang Xiao<sup>a,n,3</sup>

<sup>a</sup>Department of Physics, Tsinghua University, Beijing 100084, China;

<sup>b</sup>College of Physics and Technology, Guangxi Normal University, Guilin 541004, China;

<sup>c</sup>Guangxi Key Laboratory of Nuclear Physics and Technology, Guangxi Normal University, Guilin 541004, China;

<sup>d</sup>University of Chinese Academy of Sciences, Beijing 100049, China;

<sup>e</sup>Institute of Modern Physics, Chinese Academy of Sciences, Lanzhou 730000, China;

<sup>f</sup>School of Science, Huzhou University, Huzhou, 313000, China;

<sup>g</sup>College of Nuclear Science and Technology, Beijing Normal University, Beijing 100875, China;

<sup>h</sup>Institute of Particle and Nuclear Physics, Henan Normal University, Xinxiang 453007, China;

<sup>i</sup>Shanghai Institute of Applied Physics, Chinese Academy of Science, Shanghai 201800, China;

<sup>j</sup>Shanghai Advanced Research Institute, Chinese Academy of Science, Shanghai 201210, China;

<sup>k</sup>School of Nuclear Science and Technology, University of South China, Hengyang 421001, China;

<sup>l</sup>China Institute of Atomic Energy, Beijing 102413, China;

<sup>m</sup>Institute of Physics, Maria Curie Skłodowska University, 20-031 Lublin, Poland

<sup>n</sup>Collaborative Innovation Center of Quantum Matter, Tsinghua University, Beijing 100084, China;

---

## Abstract

The neutron rich neck zone created in heavy ion reaction is experimentally probed by the production of the  $A = 3$  isobars. The energy spectra and angular distributions of triton and  ${}^3\text{He}$  are measured with the CSHINE detector in  ${}^{86}\text{Kr} + {}^{208}\text{Pb}$  reactions at 25 MeV/u. While the energy spectrum of  ${}^3\text{He}$  is harder than that of triton, known as “ ${}^3\text{He}$ -puzzle”, the yield ratio  $R(t/{}^3\text{He})$  presents a robust rising trend with the polar angle in laboratory. Using the fission fragments to reconstruct the fission plane, the enhancement of out-plane  $R(t/{}^3\text{He})$  is confirmed in comparison to the in-plane ratios. Transport model simulations reproduce qualitatively the experimental trends, but the quantitative agreement is not achieved. The results demonstrate that a neutron rich neck zone is formed in the reactions. Further studies are called for to understand the clustering and the isospin dynamics related to neck formation.

*Key words:* Neutron rich neck,  ${}^3\text{He}$ -puzzle, out-plane emission, Isospin transport

*PACS:* 25.70.-z

---

## 1 Introduction

Heavy ion reaction (HIR) is a micro-laboratory for investigating the properties of the nuclear equation of state (nEoS), particularly the nuclear symmetry energy  $E_{\text{sym}}(\rho)$  [1,2,3,4,5,6]. The accurate constraint of  $E_{\text{sym}}(\rho)$  is crucial for both nuclear- and astro-physics, and becomes unprecedentedly important since the detection of the gravitational wave from the neutron star merging event GW170817 [7,8,9]. Although great progress has been made via the detection of isobaric yield ratios in HIRs, like  $n/p$  [10],  $t/{}^3\text{He}$  [11,12],  $\pi^-/\pi^+$  [13,14,15,16],  $K^0/K^+$  [17] and  $\Xi^-/\Xi^0$  [18], the transport model evaluation project (TMEP) has been launched to benchmark the method to allocate the uncertainties in model analysis of  $E_{\text{sym}}(\rho)$  [19,20,21,22,23], and the efforts are ongoing to search novel probes to explore the effects of  $E_{\text{sym}}(\rho)$  in HIRs [24,25,26,27].

The determination of  $E_{\text{sym}}(\rho)$  relies on the comprehensive view of the underlining dynamic process of HIRs, particularly that involving the isospin degree of freedom (IDOF) [28]. During the thermal and chemical evolution of the reaction, a low-density neutron rich neck zone is formed as the result of the complicated dynamics [29,30]. The neck zone has been explored to understand the mechanism of intermediate mass fragment formation [31,32,33,34], isotopic cluster emission [35,36,37,38] and neutron-proton equilibration [39,40,41,42,43]. Because of the

---

<sup>1</sup> E-mail: yj-wang15@tsinghua.org.cn

<sup>2</sup> E-mail: liou@gxnu.edu.cn

<sup>3</sup> E-mail: xiaozg@tsinghua.edu.cn

density gradient and the isospin migration, the neck zone provides a beneficial environment to study the  $E_{\text{sym}}(\rho)$  [41,43]. For more discussions about neck zone, one can refer to the review articles of heavy ion reactions from the experimental [29,30,44] and theoretic points of view [45,46,47,48,49].

Among the probes using the light charged particles (LCPs), the yield ratio of  $t/{}^3\text{He}$ , written as  $R(t/{}^3\text{He})$ , has been particularly identified to probe the enriched feature of isospin dynamics in HIRs. Transport model calculations demonstrate that the  $R(t/{}^3\text{He})$  at intermediate energies HIRs depends on the stiffness of  $E_{\text{sym}}(\rho)$  [12,50]. At high energy HIRs,  $R(t/{}^3\text{He})$  depends more sensitively on the value of  $E_{\text{sym}}(\rho)$  [51] and the specific form of the interaction potential [16,52], but less dependent on the slope of  $E_{\text{sym}}(\rho)$  [53]. In addition,  $R(t/{}^3\text{He})$  reflects the isospin dependent nucleon density in the reactions [54,32,55]. Experimentally, the yield ratios of various mirror nucleus pairs, including the  $R(t/{}^3\text{He})$ , led to the discovery of isospin fractionation [56]. It has been suggested that more neutron-rich particles are emitted at midrapidity, as inferred by the  $R(t/{}^3\text{He})$ , which correlates positively with the charge number of projectile-like fragments[32] but reversely with the center of mass energy [57]. Similarly, in high-energies HIR, the  $R(t/{}^3\text{He})$  reflects the neutron enrichment of the emission source[58,32,59] and isospin mixing during the collision [60]. Recently, the  $R(t/{}^3\text{He})$  has also been used to study the pick-up mechanism of pre-equilibrium light nucleus production in the pion scattering experiment [61].

Despite of the enormous progress of the studies on the triton and  ${}^3\text{He}$  emission, some questions remain unclear and require further studies. For example, when considering the spectra of  ${}^3\text{He}$ , there is an anomalous phenomenon that the yield of high energy  ${}^3\text{He}$  is relatively larger, compared to that of triton [62,63,64,65,66] or  ${}^4\text{He}$  [62,67,64,65,66]. This phenomenon has been called “ ${}^3\text{He}$ -puzzle” [62,63,66]. While the energy spectra are suffering “ ${}^3\text{He}$ -puzzle”, the yield ratio of  $t$  and  ${}^3\text{He}$  is sensitive to the neutron-to-proton ratio ( $N/Z$ ) of the emission system [59,68,42,69]. The excitation function of  $R(t/{}^3\text{He})$  measured by the FOPI collaboration [70] can not be reproduced with a single model [51]. More interestingly, the results of the INDRA experiment suggest that the  $t$  and  ${}^3\text{He}$  isobars seem to dominate the neutron enrichment of the neck zone [43].

Due to the enriched but not-well-understood information carried by triton and  ${}^3\text{He}$  coupling to both the isospin transport and the neck formation in HIRs, we are motivated to explore the emission of these two isobars by looking at the energy spectra and the yield ratio  $R(t/{}^3\text{He})$  over wide angular range, and to link the ratio to the feature of neck emissions. In this letter, the energy spectra of  $t$  and  ${}^3\text{He}$  at different angles are measured in the reactions of  ${}^{86}\text{Kr}+{}^{208}\text{Pb}$  at 25 MeV/u. The distributions of  $R(t/{}^3\text{He})$  as a function of the laboratory polar angle and of the angle with respect to the fission plane are analyzed. The comparison of the experimental data to the transport model simulation is discussed. The paper is organized as following. Section 2 and 3 present the experimental setup and the description of the transport model, respectively. Section 4 is the results and the discussions, and section 5 is the

summary.

## 2 Experimental setup

The experiment was conducted at the Compact Spectrometer for Heavy Ion Experiment (CSHINE) [71,72], built at the final focal plane of the Radioactive Ion Beam Line at Lanzhou (RIBLL-I) [73]. The  $^{86}\text{Kr}$  beam of 25 MeV/u was extracted from the cyclotron of the Heavy Ion Research Facility at Lanzhou (HIRFL) [74], bombarding a natural lead target installed in the scattering chamber with the radius  $R \approx 750$  mm. The target thickness is about  $1 \text{ mg/cm}^2$ . The LCPs from the reactions were measured by 4 silicon-strip detector telescopes (SSDTs), covering the angular range from  $10^\circ$  to  $60^\circ$  in laboratory. Each SSDT consists of three layers, namely, one single-sided silicon-strip detector (SSSSD) for  $\Delta E_1$  and one double-sided silicon strip detector (DSSSD) for  $\Delta E_2$ , backed by a  $3 \times 3$  CsI(Tl) crystal hodoscope with the length of 50 mm for the energy deposit  $E$ . The granularity of the SSDT is  $4 \times 4 \text{ mm}^2$ , giving about  $1^\circ$  angular resolution. The energy resolution of the SSDT is better than 2%, and the isotopes up to  $Z = 6$  can be identified. Multi hits and signal sharing are carefully treated in the track recognition, and the track recognition efficiency is about 90% [75]. In order to tag the reaction geometry, the fission fragments (FFs) were detected by 3 parallel plate avalanche counters (PPACs), each of which had a sensitive area of  $240 \times 280 \text{ mm}^2$ . The perpendicular distance of the PPACs to the target is about 428 mm. The coverage of the PPACs ensures a high efficiency to measure the LCPs in coincidence with the FFs selecting the semi-peripheral collisions. Fig. 1 presents the experimental setup (a) and the spatial coverage of the SSDTs and the PPACs (b).

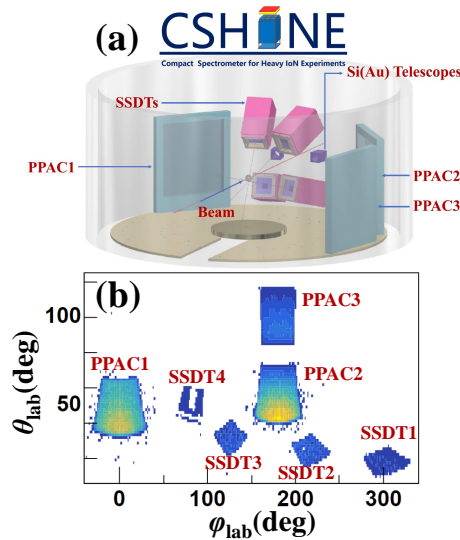


Fig. 1. (Color online) (a) The experimental setup of CSHINE. (b) The spatial coverage of SSDTs and PPACs on  $\theta - \phi$  plane in laboratory reference frame.

### 3 Theoretical Model

A hybrid model by the improved quantum molecular dynamics model (ImQMD05) coupled with statistic decay afterburner (GEMINI) was used for theoretical simulation in this work. The ImQMD05 [76] was used to simulate the nucleon transport process in HIRs. And the GEMINI [77,78] was followed to obtain the final state productions of the reactions. The ImQMD05 model is an improved version from the original quantum molecular dynamics code [79,80], and is widely used to understand the nuclear reaction dynamics by event-by-event analysis in both low and intermediate energies HIRs. The mean field part of the ImQMD05 model used here includes the symmetry potential energy part. And the local nuclear potential energy density functional in the ImQMD05 model is written as

$$V_{\text{loc}} = \frac{\alpha \rho^2}{2 \rho_0} + \frac{\beta}{\eta + 1} \frac{\rho^{\eta+1}}{\rho_0^\eta} + \frac{g_{\text{sur}}}{2\rho_0} (\nabla\rho)^2 \quad (1)$$

$$+ \frac{g_{\text{sur,iso}}}{\rho_0} [\nabla(\rho_n - \rho_p)]^2 + g_{\rho\tau} \frac{\rho^{8/3}}{\rho_0^{5/3}} + \frac{C_s}{2} \frac{\rho^{\gamma+1}}{\rho_0^\gamma} \delta^2,$$

where  $\rho$ ,  $\rho_n$ ,  $\rho_p$  are the density of nucleon, neutron, and proton, respectively.  $\delta = (\rho_n - \rho_p)/(\rho_n + \rho_p)$  is the isospin asymmetry degree. The parameters in Eq. (1) except  $C_s$ , which are listed in Table 1, are obtained directly from MSL0 parameter set [81].  $C_s$  is determined by the symmetry potential energy at saturation density. Together with various  $\gamma$ , one can get the MSL0-like Skyrme interaction with various density dependent symmetry potential energy. The reaction was simulated with impact parameter in the range of  $1.0 \leq b \leq 7.0$  fm by step of  $\Delta b = 1.5$  fm. At the end of dynamics evolution in ImQMD, the minimum spanning tree (MST) algorithm [80,82] was used to recognize the free nucleons and fragments formed in the evolution. Next, the statistical decay of excited fragments was performed with GEMINI model. At last, the information of final state particles will be obtained.

Table 1  
Parameter set used in the ImQMD calculations.

$\alpha$	$\beta$	$\eta$	$g_{\text{sur}}$	$g_{\text{sur,iso}}$	$g_{\rho\tau}$	$C_s$	$\rho_0$
(MeV)	(MeV)		(MeV fm <sup>2</sup> )	(fm <sup>2</sup> )	(MeV)	(MeV)	(fm <sup>-3</sup> )
-254	185	5/3	21.0	-0.82	5.51	36.0	0.160

## 4 Results and Discussions

We first analyze the energy spectra, which contain thermal and dynamical information of the particle emission. Fig. 2 presents the energy spectra of triton (solid squares) and  $^3\text{He}$  (open triangles) in different angular ranges corresponding to SS-DTs 2 to 4. To reduce the influence of quasi-projectiles, the data of SS-DT1 covering  $10 - 20^\circ$  in the laboratory is not counted here. It is shown that the spectrum of  $^3\text{He}$  is generally harder than that of triton, leading to a larger average kinetic energy of the former. The difference between triton and  $^3\text{He}$  is more pronounced at forward angles than at large angles. This observation of “ $^3\text{He}$ -puzzle” is in accordance with the previous measurements at high beam energies [83,62,65,84,85,66,64,86,70]. Consistently, our experimental results supports that the “ $^3\text{He}$ -puzzle” is more pronounced in the heavy system than that in light systems reported in the Fermi energy range [85,86,64].

The “ $^3\text{He}$ -puzzle” has been interpreted by two possible scenarios: sequential decay [63] and coalescence model [67]. In the sequential decay scenario, the difference between  $^3\text{He}$  and  $t$  is influenced by the Coulomb barrier, for which  $^3\text{He}$  is emitted at an earlier stage with high temperature to overcome the Coulomb barrier higher than that of  $t$  [63]. In coalescence scenario, which was applied to interpret the difference between  $^3\text{He}$  and  $\alpha$  particles [67], the former is dominantly produced by the coalescence of preequilibrium nucleons, delivering larger mean kinetic energy. These two explanations are qualitatively in agreement, suggesting that  $^3\text{He}$  is predominantly emitted at earlier stage.

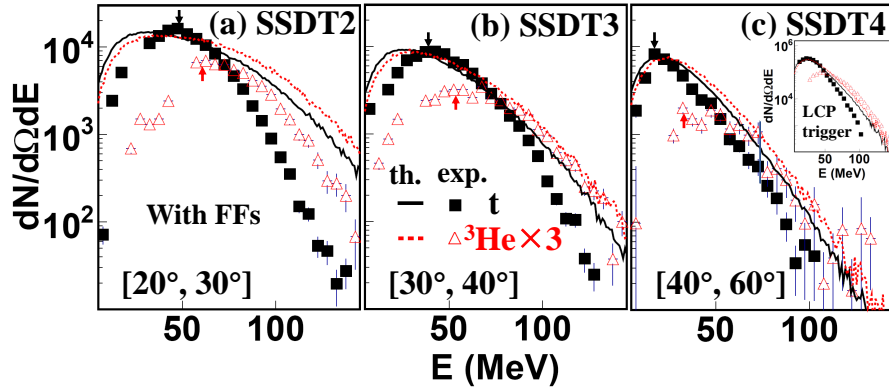


Fig. 2. (Color online) The energy spectra of triton (solid) and  $^3\text{He}$  (open) in  $20^\circ \leq \theta_{\text{lab}} \leq 60^\circ$  covered by SS-DT2 to SS-DT4 in coincidence with the FFs. The arrows represent the peak position of each energy spectrum. Displayed in the inset of panel (c) is the spectra of  $t$  and  $^3\text{He}$  with trigger condition of  $M_{\text{lcp}} \geq 2$ .

The energy spectra calculated by ImQMD05 are presented in Fig. 2 with solid and dash lines for  $t$  and  $^3\text{He}$ , respectively. It should be clarified that the yield of clusters is usually underestimated by transport model. In order to gain a clear view and direct comparison of the shape, the yields of the model predictions are scaled ac-

Table 2

Energy peak position  $E_p$  of t and  ${}^3\text{He}$  for SSdT 2 to 4.

	SSdT2	SSdT3	SSdT4
$E_p$ of t (MeV)	45	40	19
$E_p$ of ${}^3\text{He}$ (MeV)	62	58	38

cording to the experimental yields, and the correction factor is the same for triton and  ${}^3\text{He}$  in a given angular window. It can be seen that the trend of the spectra of t and  ${}^3\text{He}$  is qualitatively repeated by the model calculations. Switching from t to  ${}^3\text{He}$ , the energy spectra become slightly harder, and the energy peak positions move to the right side. At large angles, as shown in panel (b) and (c), the simulated descending tails of  ${}^3\text{He}$  spectra agree better with the data compared to that of triton, suggesting that the high-energy  ${}^3\text{He}$  is dominated by dynamic emissions. Quantitatively speaking, however, the splitting between t and  ${}^3\text{He}$  in model calculations is less pronounced than in the experimental data, particularly at smaller angles. It suggests that the origin and the formation of light clusters, as of t and  ${}^3\text{He}$ , is seemingly more complicated than the coalescence approach usually adopted by current transport models. We note here that in the ImQMD05 calculations, the fission events are hard to simulate because of its long time scale, so the events are selected by two LCPs firing in SSDTs,  $M_{\text{lcp}} \geq 2$ . By inspecting the experimental spectra under the same condition, as shown in the inset of panel (c) for example, the conclusions are not changed.

Benefiting from the wide angular coverage of the SSDTs in laboratory reference frame, the angular distribution of the isobaric yield ratio of t/ ${}^3\text{He}$  can be analyzed. To avoid the influence of the possible experimental distortion caused by the energy threshold in each SSDTs, we focus on the descending part on the right side of the energy peak. The energy peak positions ( $E_p$ ) are listed in Tab. 2. Meanwhile, using the energy condition  $E \geq E_p$  as the low limit cut, one can suppress the interference of the evaporation process and emphasize the feature of the dynamic emission.

Fig. 3 (a) presents the angular distribution of  $R(\text{t}/{}^3\text{He})$  at various conditions as a function of the polar angle in laboratory  $\theta_{\text{lab}}$ , where the geometry efficiency  $\eta_\varphi$  is plotted in Fig.3(b). In panel (a), the colored square markers are the experimental data from the events of one LCP in coincidence with two FFs after the  $E_p$  cuts are applied. The vertical error bars represent the statistic uncertainties and the colored caps represent the systematic uncertainties arising from  $\pm 1$  MeV variation of the energy  $E_p$ . It is clearly shown that the angular distribution exhibits a rising trend.

Since  $R(\text{t}/{}^3\text{He})$  is positively correlated to the  $N/Z$  of emission source [59,68,42,69], the behavior of  $R(\text{t}/{}^3\text{He})$  vs.  $\theta_{\text{lab}}$  in the wide angular range from  $20^\circ$  to  $60^\circ$  reveals a convincing picture of the evolution of IDOF. Due to the isospin diffusion and drift mechanisms [28], the neutrons favor to transport from high-density quasi-projectile region to low-density neck region, of which the neutron rich feature has been predicted by various transport model simulations [87,35,88,89,90,91,37,38,40], and

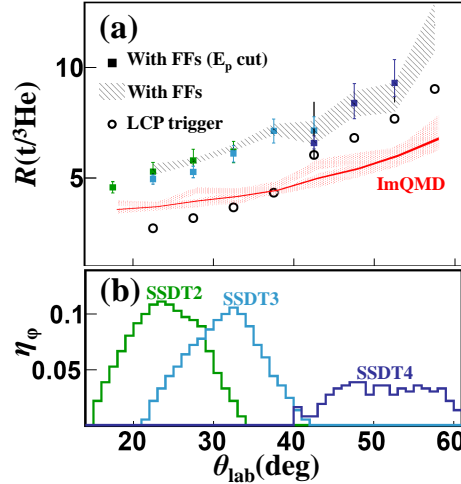


Fig. 3. (Color online) The ratio  $R(t/{}^3\text{He})$  as a function of  $\theta_{\text{lab}}$  at different conditions. The colored solid squares represent the ratio with  $E \geq E_p$  cuts in coincidence with fission events, while the diagonal hatched area represents the results by removing the  $E_p$  cuts. The open circles represents the ratio in the events triggered only by the LCPs in SSDTs with  $M_{\text{lcp}} \geq 2$ . The red solid curve and the dot-filled band is the ImQMD calculations (see text). (b) The geometric coverage efficiency  $\eta_\phi$  of SSDTs for different laboratory polar angles.

experimentally observed in a specific angular window [31,92,68,34,93,39,94,43] or a parallel velocity window [95,96,68,34,97,98,99,69,100].

The robustness of the increasing trend of  $R(t/{}^3\text{He})$  as a function of  $\theta_{\text{lab}}$  can be further checked by varying the conditions. If one takes the detector threshold as the low limit cut instead of the  $E_p$  cut, i.e.,  $v_t \geq 0.09c$  and  $v_{3\text{He}} \geq 0.15c$ , same as in [27], the ratio  $R(t/{}^3\text{He})$  increases similarly, as plotted by the diagonal hatched band in Fig. 3 (a). More interestingly, if one further removes the coincidence with two fission fragments and takes the data triggered by a minimum multiplicity of LCP  $M_{\text{lcp}}$  firing the SSDTs (in experiment  $M_{\text{lcp}} \geq 2$ ), as shown by the open circles, the increasing trend remains, but the absolute values become markedly smaller. Since SSDT2 has a much higher threshold due to the thicker  $\Delta E_1$  and  $\Delta E_2$  than SSDT 3, for the ratios without  $E_p$  cuts, only the latter is counted.

Indeed, the enhancement shown by the hatched band compared to the open circles in Fig. 3 (a) indicates that the neck emission is related to the impact parameter. In our experiment, the linear momentum transfer (LMT) derived from the folding angle of the two fission fragments is averaged at  $\langle \text{LMT} \rangle = 0.35$ . From a simple geometry picture, it corresponds to an average impact parameter  $\langle b \rangle \approx 7$  fm, which is a semi-peripheral reactions. On the other hand, the inclusive events triggered by  $M_{\text{lcp}} \geq 2$  have a much weaker  $b$  dependence. Thus, due to the overlap of the outer neutron skin of the projectile and the target, the neutron richness of the neck zone formed in the semi-peripheral events tagged by the fission fragments (diagonal hatched band) is more pronounced than in the LCP triggered events (open circles). It has been pointed out that, the neutron rich neck zone is formed from dy-



namical effects in a semi-peripheral reactions [45,88,39]. The difference between the results with and without fission tagging suggests that the neck emission occurs before the isospin equilibrium is fully achieved.

The rising trend of  $R(t/{}^3\text{He})$  is also qualitatively reproduced by transport model calculations using ImQMD05, as shown by the solid curve with dot-filled area in Fig. 3 (a). Here, the dot-filled area represents the results with  $b$  varying from 1.0 to 7.0 fm, and the solid curve is the  $b$ -averaged value. The parameter of  $E_{\text{sym}}(\rho)$  is  $\gamma = 0.5$ . The trigger and cut condition is the same as for the open circles. The calculations confirm the increasing trend but underestimate the increasing rate compared to the data points. Again, the failure of quantitative reproduction of the data suggests the complication of the clustering mechanism in heavy ion collisions at Fermi energies.

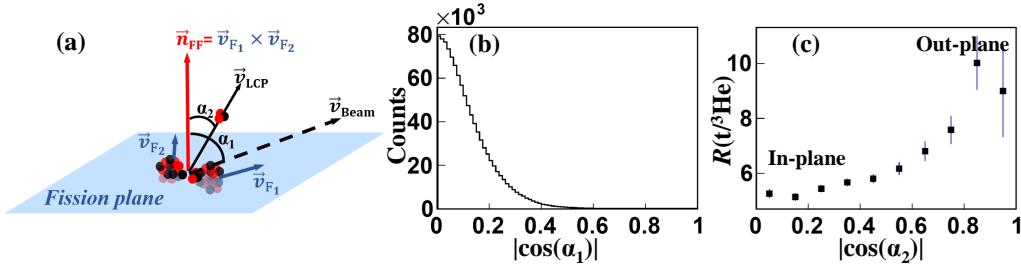


Fig. 4. (Color online) (a) Geometric diagram of fission plane of FFs and neck emission. (b) Angular distribution between the normal vector  $\vec{n}_{\text{FF}}$  of the fission plane and the beam direction  $\vec{v}_{\text{beam}}$ . (c) Angular distribution between the normal vector of the fission plane and the velocity of LCPs  $\vec{v}_{\text{LCP}}$ .

Finally, the neutron rich neck emission can be confirmed via the ratio  $R(t/{}^3\text{He})$  in and out of the fission plane, as shown in Fig. 4 (a). The fission plane is reconstructed by the velocity of two FFs, using  $\vec{n}_{\text{FF}} = (\vec{v}_{\text{F1}} \times \vec{v}_{\text{F2}}) / (|\vec{v}_{\text{F1}}||\vec{v}_{\text{F2}}|)$  to denote the normal vector of the plane. Defining  $\alpha_1$  as the angle between  $\vec{n}_{\text{FF}}$  and the beam direction  $\vec{v}_{\text{beam}}$ , the distribution of  $\alpha_1$  characterizes how much the fission plane deviates from the beam. As shown in Fig. 4(b), the  $|\cos(\alpha_1)|$  is peaked at 0 with a rather small width  $\sigma_{\alpha_1} \approx 6^\circ$ , inferring that the fission plane keeps approximately the memory of the initial angular momentum of the rotating system.

With the above inference, Fig. 4(c) presents the angular distribution of  $R(t/{}^3\text{He})$  with respect to the fission plane. The  $\alpha_2$  on the abscissa is the relative angle between  $\vec{n}_{\text{FF}}$  and the velocity of the coincident triton or  ${}^3\text{He}$   $\vec{v}_{\text{LCP}}$ , with  $|\cos(\alpha_2)| = 0$  (1) corresponding to in-plane (out-plane) emission. The  $E_p$  cuts are applied same as in Fig. 3 to calculate the  $R(t/{}^3\text{He})$ . The increasing trend of  $R(t/{}^3\text{He})$  with  $|\cos(\alpha_2)|$  indicates that the out-plane emission is enhanced. In a naive picture, the particles emitted from the neck region favor more out-plane at  $\alpha_2 \approx 0^\circ$  or  $\cos(\alpha_2) \approx 1$  because the emission in the fission plane can be blocked by the two heavy fragments. On the other hand, the particles emitted from both bodies of the dinuclear system, followed by the rupture to quasi-projectile and quasi-target, respectively, tend to populate in-plane at  $\alpha_2 \approx 90^\circ$  because of the centrifugal motion. According to

the picture, the increasing trend of  $R(t/{}^3\text{He})$  as a function of  $|\cos(\alpha_2)|$  consistently supports the formation of the neutron rich neck in the reactions.

## 5 Summary

The energy spectra and the angular distribution of triton and  ${}^3\text{He}$  ranging from  $20^\circ$  to  $60^\circ$  in the laboratory in coincidence with fission fragments are analyzed in 25 MeV/u  ${}^{86}\text{Kr} + {}^{208}\text{Pb}$  reactions. It is shown that the energy spectra of  ${}^3\text{He}$  are generally harder than triton, and the effect is more pronounced at small angles. The yield ratio  $R(t/{}^3\text{He})$  exhibits an increasing trend with  $\theta_{\text{lab}}$ , evidencing the evolution of the isospin and density gradient from quasi-projectile to the mid-velocity neck region. The ImQMD simulations achieve a qualitative description of the energy spectra and angular distribution of t and  ${}^3\text{He}$ , supporting the dynamic feature of the emission of t and  ${}^3\text{He}$  from the neck. However, the failure of quantitative reproduction, which can not be cured by the filter conditions in the analysis, indicates a more complicated clustering mechanism than the current coalescence picture in the transport model and calls for further systematic investigations. Moreover, the ratio  $R(t/{}^3\text{He})$  increases with the angle to the fission plane, in accordance with the enhancement of the out-plane emission of neutron-rich particles from the neck. The distribution properties of triton and  ${}^3\text{He}$  provide an effective means to understand isospin dynamics related to the neck formation and a fine probe to constrain the  $E_{\text{sym}}(\rho)$  in heavy ion reactions.

## 6 Acknowledgement

This work is supported by the Ministry of Science and Technology of China under Nos. 2022YFE0103400 and 2020YFE0202001, and by the National Natural Science Foundation of China under Grant Nos. 12205160, 11961131010, 11961141004, and 11965004, and by the Polish National Science Center under No. 2018/30/Q/ST2/00185. Z.G.X is also supported by Tsinghua University Initiative Scientific Research Program and the Heavy Ion Research Facility at Lanzhou (HIRFL). The authors thank Huigan Cheng from SCUT, Zhen Zhang from SYSU and Rui Wang from INFN for their valuable discussions.

## References

- [1] Bao-An Li, Bao-Jun Cai, Wen-Jie Xie, and Nai-Bo Zhang. Progress in Constraining Nuclear Symmetry Energy Using Neutron Star Observables Since GW170817. *Universe*, 7(6):182, 2021.

- [2] S. Huth et al. Constraining Neutron-Star Matter with Microscopic and Macroscopic Collisions. *Nature*, 606:276–280, 2022.
- [3] Andrew W. Steiner, Madappa Prakash, James M. Lattimer, and Paul J. Ellis. Isospin asymmetry in nuclei and neutron stars. *Phys. Rept.*, 411:325–375, 2005.
- [4] M. Oertel, M. Hempel, T. Klähn, and S. Typel. Equations of state for supernovae and compact stars. *Rev. Mod. Phys.*, 89(1):015007, 2017.
- [5] Bao-An Li, Angels Ramos, Giuseppe Verde, and Isaac Vidana. Topical issue on nuclear symmetry energy. *Eur. Phys. J. A*, 50:9, 2014.
- [6] Bao-An Li, Lie-Wen Chen, and Che Ming Ko. Recent Progress and New Challenges in Isospin Physics with Heavy-Ion Reactions. *Phys. Rept.*, 464:113–281, 2008.
- [7] B. P. Abbott et al. GW170817: Observation of Gravitational Waves from a Binary Neutron Star Inspiral. *Phys. Rev. Lett.*, 119(16):161101, 2017.
- [8] B. P. Abbott et al. GW170817: Measurements of neutron star radii and equation of state. *Phys. Rev. Lett.*, 121(16):161101, 2018.
- [9] Soumi De, Daniel Finstad, James M. Lattimer, Duncan A. Brown, Edo Berger, and Christopher M. Biwer. Tidal Deformabilities and Radii of Neutron Stars from the Observation of GW170817. *Phys. Rev. Lett.*, 121(9):091102, 2018. [Erratum: *Phys.Rev.Lett.* 121, 259902 (2018)].
- [10] Bao-An Li, C. M. Ko, and Zhong-zhou Ren. Equation of state of asymmetric nuclear matter and collisions of neutron rich nuclei. *Phys. Rev. Lett.*, 78:1644, 1997.
- [11] Ying-xun Zhang and Zhu-xia Li. Probing the density dependence of the symmetry potential with peripheral heavy-ion collisions. *Phys. Rev. C*, 71:024604, 2005.
- [12] Lie-Wen Chen, Che Ming Ko, and Bao-An Li. Light clusters production as a probe to the nuclear symmetry energy. *Phys. Rev. C*, 68:017601, 2003.
- [13] Bao-An Li. Probing the high density behavior of nuclear symmetry energy with high-energy heavy ion collisions. *Phys. Rev. Lett.*, 88:192701, 2002.
- [14] Zhigang Xiao, Bao-An Li, Lie-Wen Chen, Gao-Chan Yong, and Ming Zhang. Circumstantial Evidence for a Soft Nuclear Symmetry Energy at Suprasaturation Densities. *Phys. Rev. Lett.*, 102:062502, 2009.
- [15] J. Estee et al. Probing the Symmetry Energy with the Spectral Pion Ratio. *Phys. Rev. Lett.*, 126(16):162701, 2021.
- [16] Qingfeng Li, Zhuxia Li, Sven Soff, Marcus Bleicher, and Horst Stoecker. Probing the density dependence of the symmetry potential at low and high densities. *Phys. Rev. C*, 72:034613, 2005.
- [17] G. Ferini, T. Gaitanos, M. Colonna, M. Di Toro, and H. H. Wolter. Isospin effects on sub-threshold kaon production at intermediate energies. *Phys. Rev. Lett.*, 97:202301, 2006.

- [18] Gao-Chan Yong, Bao-An Li, Zhi-Gang Xiao, and Zi-Wei Lin. Probing high-density nuclear symmetry energy with  $\Xi^-/\Xi^0$  ratio in heavy-ion collisions at  $\sqrt{s_{NN}} \sim 3$  GeV. *Phys. Rev. C*, 106:024902, 2022.
- [19] Jun Xu. Transport approaches for the description of intermediate-energy heavy-ion collisions. *Prog. Part. Nucl. Phys.*, 106:312–359, 2019.
- [20] Yong-Jia Wang and Qing-Feng Li. Application of microscopic transport model in the study of nuclear equation of state from heavy ion collisions at intermediate energies. *Front. Phys. (Beijing)*, 15(4):44302, 2020.
- [21] Ying-Xun Zhang et al. Comparison of heavy-ion transport simulations: Collision integral in a box. *Phys. Rev. C*, 97(3):034625, 2018.
- [22] Akira Ono et al. Comparison of heavy-ion transport simulations: Collision integral with pions and  $\Delta$  resonances in a box. *Phys. Rev. C*, 100(4):044617, 2019.
- [23] Maria Colonna et al. Comparison of heavy-ion transport simulations: Mean-field dynamics in a box. *Phys. Rev. C*, 104(2):024603, 2021.
- [24] Yan Zhang et al. Long-time drift of the isospin degree of freedom in heavy ion collisions. *Phys. Rev. C*, 95(4):041602, 2017.
- [25] Li Ou, Zhigang Xiao, Han Yi, Ning Wang, Min Liu, and Junlong Tian. Dynamic Isovector Reorientation of Deuteron as a Probe to Nuclear Symmetry Energy. *Phys. Rev. Lett.*, 115(21):212501, 2015.
- [26] Yijie Wang et al. The emission order of hydrogen isotopes via correlation functions in 30 MeV/u Ar+Au reactions. *Phys. Lett. B*, 825:136856, 2022.
- [27] Yijie Wang et al. Observing the ping-pong modality of the isospin degree of freedom in cluster emission from heavy-ion reactions. *Phys. Rev. C*, 107(4):L041601, 2023.
- [28] S. Hudan and R. T. deSouza. Timescale for isospin equilibration in projectile breakup. *Eur. Phys. J. A*, 50(2):36, 2014.
- [29] G. Poggi. Neck emissions and the isospin degree of freedom. *Nucl. Phys. A*, 685:296–311, 2001.
- [30] M Di Toro, Alessandro Olmi, and R Roy. Neck dynamics. In *Dynamics and Thermodynamics with Nuclear Degrees of Freedom*, pages 65–70. Springer, 2006.
- [31] J. Toke et al. Intermediate-Mass Fragment Decay of the Neck Zone Formed in Peripheral Bi-209 + Xe-136 Collisions at Elab/A=28 MeV. *Phys. Rev. Lett.*, 75:2920–2923, 1995.
- [32] J. F. Dempsey et al. Isospin dependence of intermediate mass fragment production in heavy-ion collisions at E/A=55 MeV. *Phys. Rev. C*, 54:1710–1719, 1996.
- [33] E. Ramakrishnan, H. Johnston, F. Gimeno-Nogues, D. J. Rowland, R. Laforest, Y-W. Lui, S. Ferro, S. Vasal, and S. J. Yennello. Fragment emission from the mass-symmetric reactions Fe-58, Ni-58 + Fe-58, Ni-58 at Ebeam= Me-30V/nucleon. *Phys. Rev. C*, 57:1803–1811, 1998.

- [34] S. Hudan et al. Comparison of mid-velocity fragment formation with projectile-like decay. *Phys. Rev. C*, 71:054604, 2005.
- [35] L. G. Sobotka, J. F. Dempsey, R. J. Charity, and P. Danielewicz. Clustered and neutron-rich low density 'neck' region produced in heavy-ion collisions. *Phys. Rev. C*, 55:2109–2111, 1997.
- [36] R. Laforest, E. Ramakrishnan, D. J. Rowland, A. Ruangma, E. M. Winchester, E. Martin, and S. J. Yennello. Dependence of projectile fragmentation on target  $N/Z$ . *Phys. Rev. C*, 59:2567–2573, 1999.
- [37] YingXun Zhang, ChengShuang Zhou, JiXian Chen, Ning Wang, Kai Zhao, and ZhuXia Li. Correlation between the fragmentation modes and light charged particles emission in heavy ion collisions. *Science China Physics, Mechanics & Astronomy*, 58:1–8, 2015.
- [38] Zhao-Qing Feng. Effects of isospin dynamics on neck fragmentation in isotopic nuclear reactions. *Phys. Rev. C*, 94(1):014609, 2016.
- [39] A. Rodriguez Manso, A. B. McIntosh, A. Jedele, K. Hagel, L. Heilborn, Z. Kohley, L. W. May, A. Zarrella, and S. J. Yennello. Detailed characterization of neutron-proton equilibration in dynamically deformed nuclear systems. *Phys. Rev. C*, 95(4):044604, 2017.
- [40] Han-Sheng Wang, Jun Xu, Bao-An Li, and Wen-Qing Shen. Reexamining the isospin-relaxation time in intermediate-energy heavy-ion collisions. *Phys. Rev. C*, 98(5):054608, 2018.
- [41] R. Bougault et al. Light charged clusters emitted in 32 MeV/nucleon  $^{136,124}\text{Xe} + ^{124,112}\text{Sn}$  reactions: Chemical equilibrium and production of  $^3\text{He}$  and  $^6\text{He}$ . *Phys. Rev. C*, 97(2):024612, 2018.
- [42] L. W. May et al. Neutron-proton equilibration in 35 MeV/u collisions of  $64,70\text{Zn} + 64,70\text{Zn}$  and  $64\text{Zn}, 64\text{Ni} + 64\text{Zn}$ ,  $64\text{Ni}$  quantified using triplicate probes. *Phys. Rev. C*, 98(4):044602, 2018.
- [43] Q. Fable et al. Experimental study of isospin transport with  $\text{Ca}40,48 + \text{Ca}40,48$  reactions at 35 MeV/nucleon. *Phys. Rev. C*, 107(1):014604, 2023.
- [44] E. De Filippo and A. Pagano. Experimental effects on dynamics and thermodynamics in nuclear reactions on the symmetry energy as seen by the CHIMERA  $4\pi$  detector. *Eur. Phys. J. A*, 50:32, 2014.
- [45] V. Baran, M. Colonna, M. Di Toro, V. Greco, M. Zielinska-Pfabe, and H. H. Wolter. Isospin effects in nuclear fragmentation. *Nucl. Phys. A*, 703:603–632, 2002.
- [46] V. Baran, M. Colonna, and M. Di Toro. Neck fragmentation reaction mechanism. *Nucl. Phys. A*, 730:329–354, 2004.
- [47] V. Baran, M. Colonna, M. Di Toro, M. Zielinska-Pfabe, and H. H. Wolter. Isospin transport at Fermi energies. *Phys. Rev. C*, 72:064620, 2005.

- [48] Maria Colonna, Virgil Baran, and Massimo Di Toro. Theoretical predictions of experimental observables sensitive to the symmetry energy. *Eur. Phys. J. A*, 50:30, 2014.
- [49] Maria Colonna. Collision dynamics at medium and relativistic energies. *Progress in Particle and Nuclear Physics*, 113:103775, 2020.
- [50] Lie-Wen Chen, C. M. Ko, and Bao-An Li. Light cluster production in intermediate-energy heavy ion collisions induced by neutron rich nuclei. *Nucl. Phys. A*, 729:809–834, 2003.
- [51] Yongjia Wang, Chenchen Guo, Qingfeng Li, and Hongfei Zhang.  ${}^3\text{H}/{}^3\text{He}$  ratio as a probe of the nuclear symmetry energy at sub-saturation densities. *Eur. Phys. J. A*, 51(3):37, 2015.
- [52] T. Gaitanos, M. Colonna, M. Di Toro, and H. H. Wolter. Stopping and isospin equilibration in heavy ion collisions. *Phys. Lett. B*, 595:209–215, 2004.
- [53] Gao-Chan Yong, Bao-An Li, Lie-Wen Chen, and Xun-Chao Zhang. Triton-He-3 relative and differential flows as probes of the nuclear symmetry energy at supra-saturation densities. *Phys. Rev. C*, 80:044608, 2009.
- [54] P. Chomaz and F. Gulminelli. Phase transition in an isospin dependent lattice gas model. *Phys. Lett. B*, 447:221–226, 1999.
- [55] S. Albergo, S. Costa, E. Costanzo, and A. Rubbino. Temperature and free-nucleon densities of nuclear matter exploding into light clusters in heavy-ion collisions. *Nuovo Cim. A*, 89:1–28, 1985.
- [56] H. S. Xu et al. Isospin fractionation in nuclear multifragmentation. *Phys. Rev. Lett.*, 85:716–719, 2000.
- [57] M. A. Famiano, T. Liu, W. G. Lynch, A. M. Rogers, M. B. Tsang, M. S. Wallace, R. J. Charity, S. Komarov, D. G. Sarantites, and L. G. Sobotka. Neutron and Proton Transverse Emission Ratio Measurements and the Density Dependence of the Asymmetry Term of the Nuclear Equation of State. *Phys. Rev. Lett.*, 97:052701, 2006.
- [58] S. Nagamiya, M. C. Lemaire, E. Moller, S. Schnetzer, G. Shapiro, H. Steiner, and I. Tanihata. Production of Pions and Light Fragments at Large Angles in High-Energy Nuclear Collisions. *Phys. Rev. C*, 24:971–1009, 1981.
- [59] M. Veselsky, R. W. Ibbotson, R. Laforest, E. Ramakrishnan, D. J. Rowland, A. Ruangma, E. M. Winchester, E. Martin, and S. J. Yennello. Isospin dependence of isobaric ratio  $Y(\text{H-3}) / Y(\text{He-3})$  and its possible statistical interpretation. *Phys. Lett. B*, 497:1–7, 2001.
- [60] F. Rami et al. Isospin tracing: A Probe of nonequilibrium in central heavy ion collisions. *Phys. Rev. Lett.*, 84:1120–1123, 2000.
- [61] Yu. B. Gurov, L. Yu. Korotkova, S. V. Lapushkin, R. V. Pritula, B. A. Chernyshev, and T. D. Schurenkova. Yields of triton and  ${}^3\text{He}$  produced by nuclei in reactions of stopped pion absorption. *Bull. Russ. Acad. Sci. Phys.*, 78(11):1112–1116, 2014.

- [62] G. Poggi et al. Evidence for collective expansion in light-particle emission following Au+Au collisions at 100, 150 and 250 A·MeV. *Nucl. Phys. A*, 586(4):755–776, 1995.
- [63] R Bougault, P Eudes, D Gourio, O Tirel, E Plagnol, C Volant, T Reposeur, CO Bacri, JL Charvet, N Le Neindre, et al. A possible scenario for the time dependence of the multifragmentation process in  $xe + sn$  collisions: an explanation of the  ${}^3he$  puzzle. Technical report, SCAN-9709121, 1997.
- [64] T. X. Liu et al. Isospin observables from fragment energy spectra. *Phys. Rev. C*, 86:024605, 2012.
- [65] M. A. Lisa et al. Radial flow in Au + Au collisions at  $E = 0.25\text{-A/GeV} - 1.15\text{-A/GeV}$ . *Phys. Rev. Lett.*, 75:2662–2665, 1995.
- [66] A Bonasera, M Bruno, CO Dorso, and PF Mastinu. Critical phenomena in nuclear fragmentation. *La Rivista del Nuovo Cimento*, 23:1–101, 2000.
- [67] W. Neubert and A. S. Botvina. What is the physics behind the He-3 - He-4 anomaly? *Eur. Phys. J. A*, 7:101–106, 2000.
- [68] D. V. Shetty et al. Intermediate mass fragments and isospin dependence in Sn-124, xe-124 + Sn-124, Sn-112 reactions at 28-MeV/nucleon. *Phys. Rev. C*, 68:054605, 2003.
- [69] S. Piantelli et al. Isospin transport phenomena for the systems  ${}^{80}\text{Kr}+{}^{40,48}\text{Ca}$  at 35 MeV/nucleon. *Phys. Rev. C*, 103(1):014603, 2021.
- [70] W. Reisdorf et al. Systematics of central heavy ion collisions in the 1A GeV regime. *Nucl. Phys. A*, 848:366–427, 2010.
- [71] Fenhai Guan et al. A Compact Spectrometer for Heavy Ion Experiments in the Fermi energy regime. *Nucl. Instrum. Meth. A*, 1011:165592, 2021.
- [72] Yi-Jie Wang et al. CSHINE for studies of HBT correlation in Heavy Ion Reactions. *Nucl. Sci. Tech.*, 32(1):4, 2021.
- [73] Z. Sun, W.-L. Zhan, Z.-Y. Guo, G. Xiao, and J.-X. Li. Ribll, the radioactive ion beam line in lanzhou. *Nuclear Instruments and Methods in Physics Research Section A: Accelerators, Spectrometers, Detectors and Associated Equipment*, 503(3):496–503, 2003.
- [74] J.W. Xia, W.L. Zhan, B.W. Wei, Y.J. Yuan, M.T. Song, W.Z. Zhang, X.D. Yang, P. Yuan, D.Q. Gao, H.W. Zhao, X.T. Yang, G.Q. Xiao, K.T. Man, J.R. Dang, X.H. Cai, Y.F. Wang, J.Y. Tang, W.M. Qiao, Y.N. Rao, Y. He, L.Z. Mao, and Z.Z. Zhou. The heavy ion cooler-storage-ring project (hirfl-csr) at lanzhou. *Nuclear Instruments and Methods in Physics Research Section A: Accelerators, Spectrometers, Detectors and Associated Equipment*, 488(1):11–25, 2002.
- [75] Fenhai Guan et al. Track recognition for the  $\Delta E$ -E telescopes with silicon strip detectors. *Nucl. Instrum. Meth. A*, 1029:166461, 2022.
- [76] Yingxun Zhang, Ning Wang, Qing-Feng Li, Li Ou, Jun-Long Tian, Min Liu, Kai Zhao, Xi-Zhen Wu, and Zhu-Xia Li. Progress of quantum molecular dynamics model and its applications in heavy ion collisions. *Front. Phys. (Beijing)*, 15:54301, 2020.

- [77] R. J. Charity et al. Systematics of complex fragment emission in niobium-induced reactions. *Nucl. Phys. A*, 483:371–405, 1988.
- [78] R. J. Charity et al. Emission of unstable clusters from hot Yb compound nuclei. *Phys. Rev. C*, 63:024611, 2001.
- [79] J. Aichelin et al. Qmd versus buu/vuu. same results from different theories. *Physics Letters B*, 224:34–39, 1989.
- [80] J. Aichelin. “Quantum” molecular dynamics—a dynamical microscopic n-body approach to investigate fragment formation and the nuclear equation of state in heavy ion collisions. *Physics Reports*, 202(5-6):233–360, 1991.
- [81] Lie-Wen Chen, Che Ming Ko, Bao-An Li, and Jun Xu. Density slope of the nuclear symmetry energy from the neutron skin thickness of heavy nuclei. *Phys. Rev. C*, 82:024321, 2010.
- [82] Yingxun Zhang, Zhuxia Li, Chengshuang Zhou, and M. B. Tsang. Effect of isospin-dependent cluster recognition on the observables in heavy ion collisions. *Phys. Rev. C*, 85:051602, May 2012.
- [83] H. H. Gutbrod, A. Sandoval, P. J. Johansen, Arthur M. Poskanzer, J. Gosset, W. G. Meyer, G. D. Westfall, and R. Stock. Final State Interactions in the Production of Hydrogen and Helium Isotopes by Relativistic Heavy Ions on Uranium. *Phys. Rev. Lett.*, 37:667–670, 1976.
- [84] W. Reisdorf et al. Central collisions of Au on Au at 150, 250 and 400 MeV/nucleon. *Nucl. Phys. A*, 612:493–556, 1997.
- [85] H. Xi et al. Examining the cooling of hot nuclei. *Phys. Rev. C*, 57:R462–R465, 1998.
- [86] Ad. R. Raduta, E. Bonnet, B. Borderie, N. Le Neindre, S. Piantelli, and M. F. Rivet. Break-up stage restoration in multifragmentation reactions. *Eur. Phys. J. A*, 32:175–182, 2007.
- [87] L. G. Sobotka. Simulations of collisions between nuclei at intermediate energy using the Boltzmann-Uehling-Uhlenbeck equation with neutron skin producing potentials. *Phys. Rev. C*, 50:R1272–R1275, 1994.
- [88] R. Lioni, V. Baran, M. Colonna, and M. Di Toro. Isospin dynamics in fragmentation reactions at Fermi energies. *Phys. Lett. B*, 625:33, 2005.
- [89] V. Baran, M. Colonna, V. Greco, and M. Di Toro. Reaction dynamics with exotic beams. *Phys. Rept.*, 410:335–466, 2005.
- [90] D. D. S. Coupland, W. G. Lynch, M. B. Tsang, P. Danielewicz, and Yingxun Zhang. Influence of Transport Variables on Isospin Transport Ratios. *Phys. Rev. C*, 84:054603, 2011.
- [91] V. Baran, M. Colonna, M. Di Toro, and R. Zus. From multifragmentation to neck fragmentation: Mass, isospin, and velocity correlations. *Phys. Rev. C*, 85:054611, 2012.



- [92] L. G. Sobotka, R. J. Charity, D. K. Agnihotri, W. Gawlikowicz, T. X. Liu, W. Lynch, U. Schroder, J. Toke, and H. S. Xu. Neutron-proton asymmetry of the midvelocity material in an intermediate-energy heavy ion collision. *Phys. Rev. C*, 62:031603, 2000.
- [93] S. Piantelli, P. R. Maurenzig, A. Olmi, L. Bardelli, M. Bini, G. Casini, A. Mangiarotti, G. Pasquali, G. Poggi, and A. A. Stefanini. Distinctive features of Coulomb-related emissions in peripheral heavy ion collisions at Fermi energies. *Phys. Rev. C*, 76:061601, 2007.
- [94] E. Vient et al. New “3D calorimetry” of hot nuclei. *Phys. Rev. C*, 98(4):044611, 2018.
- [95] E. Plagnol et al. Onset of midvelocity emissions in symmetric heavy ion reactions. *Phys. Rev. C*, 61:014606, 2000.
- [96] S. Piantelli, L. Bidini, G. Poggi, M. Bini, G. Casini, P. R. Maurenzig, A. Olmi, G. Pasquali, A. A. Stefanini, and N. Taccetti. Intermediate Mass Fragment Emission Pattern in Peripheral Heavy-Ion Collisions at Fermi Energies. *Phys. Rev. Lett.*, 88:052701, 2002.
- [97] D. Theriault et al. Neutron to proton ratios of quasiprojectile and midrapidity emission in the Zn-64 + Zn-64 reaction at 45-MeV/nucleon. *Phys. Rev. C*, 74:051602, 2006.
- [98] R. Planeta et al. Centrality dependence of isospin effect signatures in Sn-124 + Ni-64 and Sn-112 + Ni-58 reactions. *Phys. Rev. C*, 77:014610, 2008.
- [99] Z. Kohley et al. Transverse collective flow and midrapidity emission of isotopically identified light charged particles. *Phys. Rev. C*, 83:044601, 2011.
- [100] R. Ogul, A. S. Botvina, M. Bleicher, N. Buyukcizmeci, A. Ergun, H. Imal, Y. Leifels, and W. Trautmann. Isospin compositions of correlated sources in the Fermi energy domain. *Phys. Rev. C*, 107(5):054606, 2023.